

Mechanisms of Peroxynitrite Decomposition Catalyzed by FeTMPS, a Bioactive Sulfonated Iron Porphyrin

Roman Shimanovich and John T. Groves¹

Department of Chemistry, 203 Hoyt Laboratory, Princeton University, Princeton, New Jersey

Received September 26, 2000, and in revised form November 17, 2000; published online February 16, 2001

Peroxynitrite is a known cytotoxic agent that plays a role in many pathological conditions. Various peroxynitrite decomposition catalysts and pathways are being explored to develop efficient therapeutic agents that can safely remove peroxynitrite from cells and tissues. Water-soluble porphyrins, such as iron(III) *meso*-tetra(2,4,6-trimethyl-3,5-disulfonato)porphine chloride (FeTMPS) and iron(III) *meso*-tetra(*N*-methyl-4-pyridyl)porphine chloride (FeTMPyP), have been shown to react catalytically with peroxynitrite (ONOO⁻). However, their mechanisms are yet to be fully understood. In this study, we have explored the reactivity of FeTMPS in the catalytic decomposition of peroxynitrite. The mechanism of this complex process has been determined. According to this mechanism, Fe(III)TMPS is oxidized by peroxynitrite to produce oxoFe(IV)TMPS and NO₂ ($k_1 = 1.3 \times 10^5 \text{ M}^{-1}\text{s}^{-1}$). The porphyrin is then reduced back to Fe(III)TMPS by nitrite, but this rate ($k_2 = 1.4 \times 10^4 \text{ M}^{-1}\text{s}^{-1}$) is not sufficient to maintain the catalytic process at the observed rate. The overall rate of peroxynitrite decomposition catalysis, k_{cat} , was determined to be $6 \times 10^4 \text{ M}^{-1}\text{s}^{-1}$, under typical conditions. We have postulated that an additional reduction pathway must exist. Kinetic simulations showed that a reaction of oxoFe(IV)TMPS with NO₂ ($k_3 = 1.7 \times 10^7 \text{ M}^{-1}\text{s}^{-1}$) could explain the behavior of this system and account for the fast reduction of oxoFe(IV)TMPS to Fe(III). Using the kinetic simulation analysis, we have also shown that two other rearrangement reactions, involving FeTMPS and peroxynitrite, are plausible pathways for peroxynitrite decay. A “cage-return” reaction between the generated oxoFe(IV)TMPS and NO₂ ($k_8 = 5.4 \times 10^4 \text{ M}^{-1}\text{s}^{-1}$), affording Fe(III)TMPS and nitrate, and a reaction between oxoFe(IV)TMPS and peroxynitrite ($k_7 = 2.4 \times 10^4 \text{ M}^{-1}\text{s}^{-1}$) that affords oxoFe(IV)TMPS and nitrate are presented. The mechanism of FeTMPS-

catalyzed peroxynitrite decay differs markedly from that of FeTMPyP, providing some insight into the reactivity of metal centers with peroxynitrite and biologically important radicals such as NO₂. © 2001 Academic Press

Key Words: peroxynitrite; iron porphyrin; nitrogen dioxide; catalysis; oxidation.

The chemistry and biology of peroxynitrite (ONOO⁻) have been under intense scrutiny since the cytotoxic activity (1–8) of this species was first recognized. In particular, reactivity toward metal centers (9–12), sulfhydryls (13, 14), and phenols (15–17) has implicated peroxynitrite in a number of pathogenic conditions (3, 8, 18–21). Endogenous reducing agents such as ascorbate and glutathione react too slowly with peroxynitrite to afford protection (14). Likewise, while the recently discovered reaction of peroxynitrite with dissolved carbon dioxide provides an additional pathway for its decomposition (22, 23), this pathway is also slow with respect to transmembrane diffusion (24) and reactions with metal centers (25). Various peroxynitrite decomposition pathways (26–29) and catalysts that mediate these processes (19, 30, 31) have become an important issue. Since peroxynitrite reacts very efficiently with biological metal centers, metalloporphyrins have been investigated as candidates for peroxynitrite decomposition catalysts (32–35). Several water-soluble iron and manganese porphyrins have shown very high rates of reaction with peroxynitrite (5). Studies in animals have shown, for example, that one such porphyrin, FeTMPS,² is able to reduce carrageenan-induced paw edema very effectively at micromolar lev-

¹ To whom correspondence and reprint requests should be addressed. Fax: (609) 258-0348. E-mail: jtgroves@princeton.edu.

² Abbreviations used: FeTMPS, iron(III) *meso*-tetra(2,4,6-trimethyl-3,5-disulfonato)porphine chloride; FeTMPyP, iron(III) *meso*-tetra(*N*-methyl-4-pyridyl)porphine chloride; Mn(III)TMPyP, manganese(III) *meso*-tetra(*N*-methyl-4-pyridyl)porphine chloride.

els and cause reductions in TNF- α and IL-1 β levels (30, 31). Since the only known reaction of FeTMPS *in vivo* is with peroxynitrite, we set out to study how this porphyrin reacts with peroxynitrite. The results of our kinetic and mechanistic studies presented here show that FeTMPS reacts with peroxynitrite in a more complex manner than cationic porphyrins such as MnTMPyP and FeTMPyP (30, 31, 33, 35).

MATERIALS AND METHODS

Materials. 5,10,15,20-Tetrakis(2,4,6-trimethyl-3,5-disulfonato)porphinatoiron-(III) chloride (Fe(III)TMPS(Cl)) was a generous gift from Dr. Stern (Monsanto Co.). Later samples were synthesized by the published procedure. Potassium persulfate, KHSO₅ (commercially available as Oxone), anhydrous monosodium phosphate, and anhydrous disodium phosphate were purchased from Aldrich. Sodium nitrite, aqueous hydrochloric acid, and sodium hydroxide were obtained from AlfaAesar. All solvents were analytical grade. Water used in all experiments was distilled and deionized (Millipore, Milli-Q).

Peroxyntirite synthesis. Peroxyntirite was prepared from the reaction of sodium nitrite with acidified hydrogen peroxide following the published procedure (38). Due to variations in the initial ONOO⁻ concentrations among various batches, the nitrite impurity was 10–30% of the peroxyntirite concentration in fresh preparations, but could be substantially higher, especially in older stock solutions, as determined by Greiss assay (see below).

Nitrite determination. Residual nitrite in the stock peroxyntirite solutions was determined spectrophotometrically, using Greiss Reagent (40). Briefly, 2 μ l of stock peroxyntirite solution was decomposed in 1 ml of pH 7.4 phosphate buffer. Then 500 μ l of the decomposed solution was mixed with 500 μ l of Greiss reagent (1 part 0.1% naphthylethyl diamine hydrochloride in H₂O to 1 part sulfonylamide in 5% phosphoric acid). Upon mixing, the reagent turned purple. After 10 min of incubation, an UV-Vis spectrum was taken and change in absorbance at 590 nm was recorded. The reagent was previously calibrated with standard nitrite solutions and the following ratio was obtained 0.04 $\Delta A_{590}/1 \mu$ M nitrite. Decay of peroxyntirite at pH 7.4 yields ~30% nitrite (49). Therefore, residual nitrite concentration was determined by subtracting the nitrite formed during the decay from total nitrite.

Time-resolved visible spectra. All reactions were carried out in 100 mM phosphate buffer at pH 7.4 and 25°C by observing changes in the peroxyntirite absorbance at 302 nm. All the time-resolved spectra were recorded on Hi-Tech SF-61 DX2 Rapid-Mixing Stopped-Flow Spectrophotometer, using photodiode array fast-scan mode. The spectral resolution was about 1 nm. Reactions between Fe(III)TMPS and peroxyntirite were single-mixing experiments and the concentrations presented in all cases are the final concentrations after mixing. The porphyrin solutions were buffered by 100 mM sodium phosphate, pH 7.4.

Reaction kinetics. Reaction kinetic profiles were collected in the photomultiplier mode on the Hi-Tech SF-61 DX2 Rapid-Mixing Stopped-Flow Spectrophotometer, using single mixing mode. The decay of peroxyntirite was monitored at 302 nm. The generation and decay of intermediates was followed at 426 nm.

Visible spectra. The electronic absorption spectra were obtained on HP 8452A Diode Array spectrophotometer.

Computer simulations and data analysis. Kinetic data was analyzed and fitted on KinetAssyst software provided by Hi-Tech. Calculations and data treatment were performed using Microsoft Excel 97. Chemical Kinetics Simulator 1.0.1 from IBM was used to perform kinetic simulations on Dell OptiPlexG1 computer. A typical simulation was performed on a system containing 10⁶ molecules to minimize noise. The state of the system, i.e., concentration of all compo-

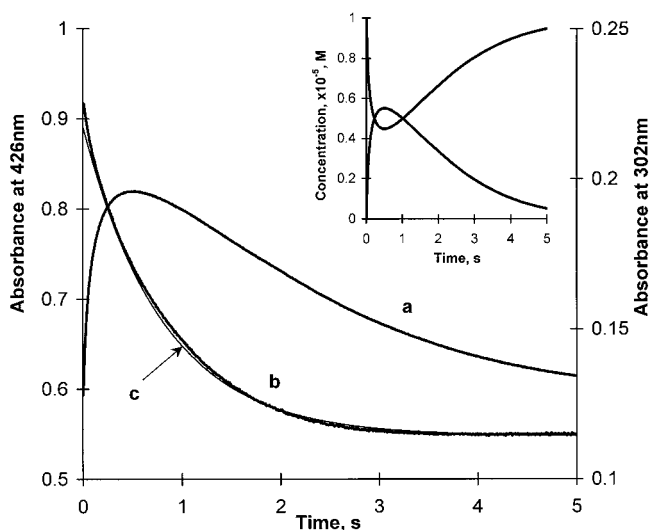


FIG. 1. Catalytic decomposition of peroxyntirite in the presence of FeTMPS. The reaction of 66 μ M peroxyntirite with 10 μ M FeTMPS was carried out at pH 7.6 at 25°C in 100 mM phosphate buffer. Trace (a) shows changes of FeTMPS to and from +3/+4 oxidation states as monitored at 426 nm. Trace (b) shows changes in the concentration of peroxyntirite that were monitored at 302 nm. An estimate of the catalytic rate constant was made by fitting the curve to a single exponential, treating reaction as a pseudo-first order in peroxyntirite with a k_{obs} of 1.23 s⁻¹, $R^2 = 0.999$, shown by trace (c). This value translates into $k_{\text{cat}} = 1.23 \times 10^5 \text{ M}^{-1}\text{s}^{-1}$, which two orders of magnitude greater than the value obtained at higher peroxyntirite concentrations in Fig. 2. Inset: Deconvolution of the trace at 426 nm into changes in the concentrations of Fe^{III} (upper trace) and oxoFe^{IV} (lower trace) over time.

nents, was recorded every 100 collision events. The simulations were initiated by a random number seed and were carried out until concentrations of all components were unchanging. The changes in concentrations of FeTMPS and peroxyntirite were converted to absorbance changes using appropriate extinction coefficients.

Modeling was also performed using EPISODE package of Scientist Version 2.0, commercial software developed by Micromath, Inc. The mathematical model was fitted, simultaneously, to FeTMPS and peroxyntirite decay data sets. The goodness of fit was evaluated using several statistical functions, including nonlinear R -squared and covariance.

RESULTS

Catalytic decay of peroxyntirite. We have studied the decomposition kinetics of peroxyntirite in the presence of FeTMPS. In the absence of the catalyst, peroxyntirite decomposes with a half-life of ~3 s (29) under the conditions employed. This spontaneous decay was nearly first-order when the concentrations did not exceed 100 μ M and was complete after 10 s. The presence of micromolar amounts of FeTMPS accelerated the observed rate of peroxyntirite decay. When 10 μ M FeTMPS was added to a solution of 66 μ M peroxyntirite, the decay of peroxyntirite occurred with a half-life of about 0.56 s, as can be seen in Fig. 1. Although the peroxyntirite decay profile could be fitted to a sin-

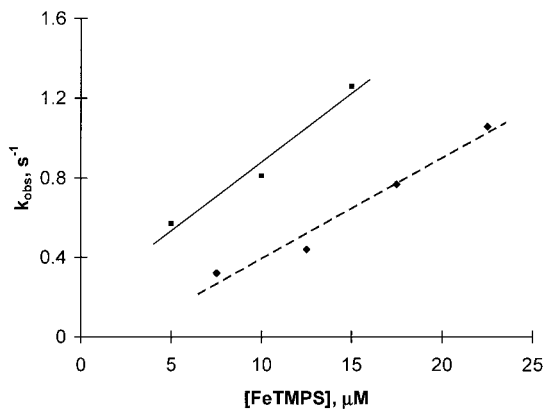


FIG. 2. Determination of k_{cat} of FeTMPs towards peroxynitrite decomposition. The observed rate constant of peroxynitrite decay was plotted against the FeTMPs concentration, when the initial peroxynitrite concentration was maintained at $\sim 260 \mu\text{M}$ (dashed line) and $\sim 220 \mu\text{M}$ (solid line). The slope of the line gives a k_{cat} value of $5.1 \times 10^4 \text{ M}^{-1}\text{s}^{-1}$ and $6.9 \times 10^4 \text{ M}^{-1}\text{s}^{-1}$, respectively.

gle exponential in this case, as shown in Fig. 1, the pseudo-first-order treatment of the reaction could not be applied here since the concentration of peroxynitrite was not sufficiently constant over the course of the reaction. In order to assess the efficiency of the catalyst in terms of k_{cat} and to be consistent throughout, we fit the first 5 s of decay to a single exponential. In separate experiments, the observed pseudo-first-order rate constant for the peroxynitrite decay was measured for three different concentrations of FeTMPs, while peroxynitrite concentration was maintained at nearly the same level. The slope of k_{obs} vs FeTMPs concentration gave an average k_{cat} value of $6.0 \times 10^4 \text{ M}^{-1}\text{s}^{-1}$ at 25°C , as can be seen in Fig. 2. However, at lower peroxynitrite concentrations, a higher value for k_{cat} is obtained as seen in Fig. 1c. The overall turnover rate of this catalyst was modest when compared to other metalloporphyrins that have been studied (36). Changes in the catalyst were also observed over the course of the reaction. As shown in Fig. 1, the absorbance of the catalyst changed during the reaction, but returned to its initial value at the end. This indicates a catalytic process during which FeTMPs was not consumed (Fig. 1, inset).

Accumulation of oxoFe(IV)TMPS during catalysis. The inventory of the catalyst was monitored by photodiode array spectroscopy over the course of peroxynitrite decomposition (Fig. 3). Fe(III)TMPS exists as a mixture of hydroxyaquaFe(III) and diaquaFe(III) complexes at pH 7.4 (37). This is signified by the presence of a shoulder of the Soret band, seen in Fig. 3. Spectroscopic titration of FeTMPs determined the $\text{p}K_{\text{a}}$ of the ligated water to be 7.1. The hydroxyaqua species has a Soret maximum at 418 nm, while the protonated form has a maximum at 398 nm. The rate of protona-

tion exchange is certainly very fast, so the two forms are in rapid equilibrium (37). Accordingly, we did not distinguish between the two forms in our kinetic treatment of the catalyst.

Reaction of Fe(III)TMPS with peroxynitrite caused a red shift in the Soret peak that is characteristic of formation of an oxoFe(IV) species as reported by Stern *et al.* (36). To confirm this finding, the oxoFe(IV) species was generated independently by stoichiometric oxidation with Oxone, shown in the inset of Fig. 3 (35). Since the extinction coefficients of oxoFe(IV)TMPS and Fe(III)TMPS at 426 nm are substantially different, monitoring at 426 nm allowed the direct observation of changes in the oxidation state of the porphyrin. The values of the extinction coefficients of these two porphyrin forms allowed a deconvolution of the changes in absorbance into changes in the concentrations of two species (Fig. 3, inset). The yields of oxoFe(IV) varied, depending on the initial concentration of peroxynitrite. The maximum yield of oxoFe(IV) in a typical reaction, where ONOO^- was $66 \mu\text{M}$, was 55%. Complete conversion of the porphyrin to the oxidized Fe(IV) form was never observed and it took several turnovers of ONOO^- over 0.5 s to reach the 55/45 Fe(IV)/Fe(III) catalyst ratio under the conditions used.

The initial rates method was used to determine the rate of oxidation of Fe(III) to Fe(IV) by peroxynitrite because the level of oxoFe(IV)TMPS began to decay at an appreciable rate shortly after its maximum concentration is reached. The initial rate of change of oxoFe(IV), was obtained by a linear fit of the first several

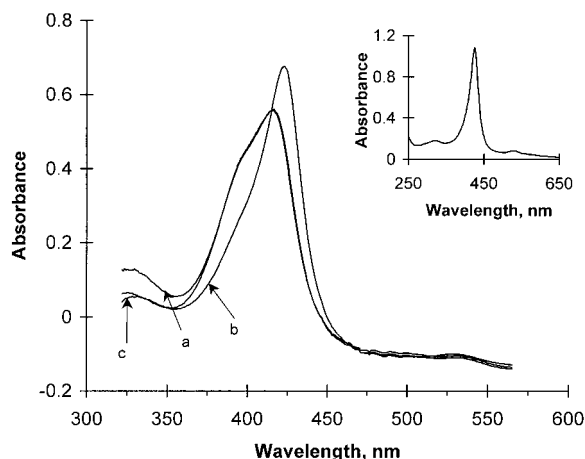


FIG. 3. Diode array spectra of catalytic peroxynitrite decomposition of FeTMPs. Trace (a) is of spectrum at $t = 0 \text{ s}$, showing only Fe^{III} and ONOO^- present. Trace (b) is of spectrum at $t = 0.5 \text{ s}$, showing FeTMPs as mainly oxoFe^{IV} and essentially no ONOO^- left. Trace (c) is of spectrum at $t = 20 \text{ s}$, showing restored Fe^{III}TMPS at the end of the reaction. Inset: Visible spectrum of oxoFe^{IV}TMPS at pH 7.4, 25°C , in 100 mM phosphate buffer, generated by adding 1 eq of Oxone to the solution of Fe^{III}TMPS. λ_{max} of Fe^{III}TMPS is 416 nm, $\epsilon_{416} = 8.35 \times 10^4 \text{ M cm}^{-1}$, $\epsilon_{426} = 6.7 \times 10^4 \text{ M cm}^{-1}$, λ_{max} of oxoFe^{IV}TMPS is 426 nm, $\epsilon_{426} = 1.08 \times 10^5 \text{ M cm}^{-1}$.

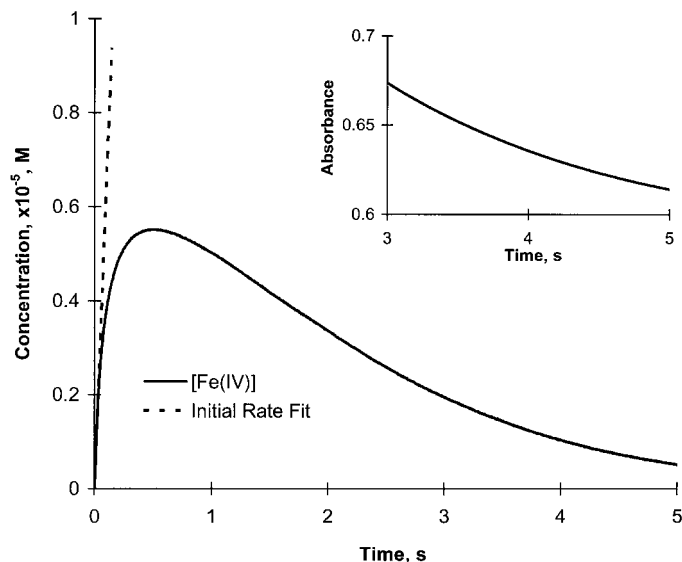


FIG. 4. Determination of the initial rate of Fe^{III} oxidation by ONOO^- . The absorbance at 426 nm was resolved into changes in Fe^{III} and oxo Fe^{IV} concentrations (oxo Fe^{IV} trace shown). The first six data points, representing 0.03 s of the reaction were subjected to a linear fit, which gave an initial rate of 6.6 M/s, $R^2 = 0.995$. Since the initial concentrations were 66 μM peroxyxynitrite and 10 μM FeTMPS , the second-order rate constant, derived from that, is $1 \times 10^5 \text{ M}^2/\text{s}$. Inset: Determination of the rate constant of reduction of oxo Fe^{IV} by nitrite in a reaction of 66 μM peroxyxynitrite with 10 μM FeTMPS . The decay in absorbance at 426 nm was fitted to a single exponential during the last 2 s of the reaction, when peroxyxynitrite has been completely decomposed. Rate of the reaction was 0.546 s^{-1} , $R^2 = 0.9998$. Since the level of nitrite was estimated at 20 μM , the second-order rate constant was calculated to be $\sim 2 \times 10^4 \text{ M}^{-1}\text{s}^{-1}$ in agreement with the value obtained by Stern *et al.* (36).

points, shown in Fig. 4, and the rate constant of oxo $\text{Fe}(\text{IV})\text{TMPS}$ formation, k_1 , was determined to be $1 \times 10^5 \text{ M}^{-1}\text{s}^{-1}$ under the conditions employed.

Reduction of oxo $\text{Fe}(\text{IV})\text{TMPS}$ by nitrite and hydrogen peroxide. The oxo $\text{Fe}(\text{IV})\text{TMPS}$ species was reduced to $\text{Fe}(\text{III})$ over several seconds after depletion of the peroxyxynitrite (Figs. 1 and 4). Since, at this point, the only reactive species in the solution are oxo $\text{Fe}(\text{IV})\text{TMPS}$ and nitrite, we suspected that the reduction of oxo $\text{Fe}(\text{IV})$ as carried out by nitrite. Nitrite ion can be present in peroxyxynitrite as a result of the method of synthesis from hydrogen peroxide and nitrite (38, 39). Further, nitrite can be formed from nitrogen dioxide, produced during the oxidation of $\text{Fe}(\text{III})\text{TMPS}$ by peroxyxynitrite. We estimated the residual nitrite concentration in peroxyxynitrite solution by Greiss assay (40).

The knowledge of the residual nitrite concentrations allowed us to estimate the rate constant for nitrite reduction of oxo $\text{Fe}(\text{IV})$. As shown in Fig. 4, we fitted the decay of oxo $\text{Fe}(\text{IV})$ after ONOO^- was gone to a single exponential expression and obtained an observed first-order rate constant of 0.55 s^{-1} . Given the estimate of the initial nitrite concentration in a 66 μM ONOO^- to

be $\sim 20 \mu\text{M}$, second order rate constant for reduction of oxo $\text{Fe}(\text{IV})$ by nitrite, k_2 , equals $\sim 2 \times 10^4 \text{ M}^{-1}\text{s}^{-1}$ for this reaction, which is consistent with the literature value (41). This shows that nitrite can reduce oxo $\text{Fe}(\text{IV})\text{TMPS}$ back to $\text{Fe}(\text{III})\text{TMPS}$ at an appreciable rate.

Since hydrogen peroxide is also present in peroxyxynitrite preparations as an impurity, its reactions with FeTMPS were evaluated. Using the stopped flow apparatus, we have measured both the oxidation rate of $\text{Fe}(\text{III})\text{TMPS}$ by H_2O_2 and the rate of reaction of H_2O_2 with oxo $\text{Fe}(\text{IV})\text{TMPS}$ and found these to be 240 and 10 $\text{M}^{-1}\text{s}^{-1}$, respectively.

We also looked at the dependence of the catalytic rate of peroxyxynitrite decay on nitrite concentration. As shown in Fig. 5, as the initial concentration of nitrite in the reaction mixture increased, the observed rate of ONOO^- decay also increased. However, the rate dependence on nitrite was very small, only a factor of two when added nitrite was increased from zero to 500 μM .

Stoichiometric reaction of $\text{Fe}(\text{III})\text{TMPS}$ with peroxyxynitrite. The reaction between peroxyxynitrite and FeTMPS was also carried out under near stoichiometric conditions. In this case, 10 μM porphyrin was reacted with 16 μM peroxyxynitrite and changes in absorbance at 302 and 426 nm were observed (Fig. 7). The maximum yield of oxo $\text{Fe}(\text{IV})$ in this case was 32%. We fitted the last 2 s of decay at 426 nm, which represented the reduction of oxo $\text{Fe}(\text{IV})$ to $\text{Fe}(\text{III})$, to a single exponential and obtained a pseudo-first order rate constant of 0.6 s^{-1} . The nitrite concentration was estimated from this rate to be $\sim 30 \mu\text{M}$.

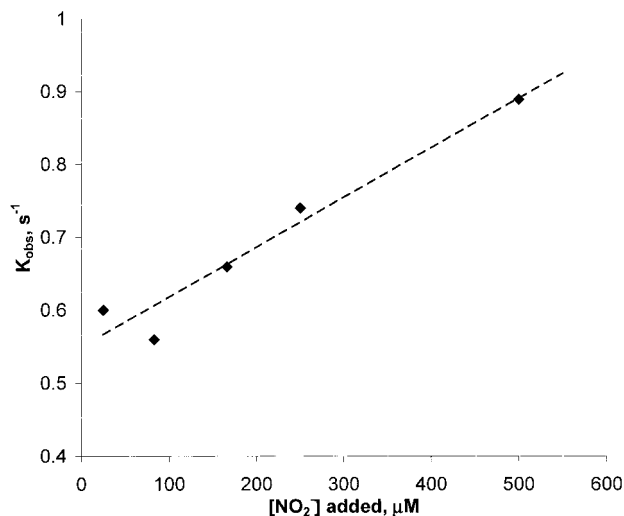


FIG. 5. Dependence of the observed first-order rate constant of peroxyxynitrite decay on the concentration of added nitrite. k_{obs} was obtained from first-order fit of absorbance decay at 302 nm. FeTMPS was 10 μM , and peroxyxynitrite was 155–205 μM at pH 7.6, 25°C, in 100 mM phosphate.

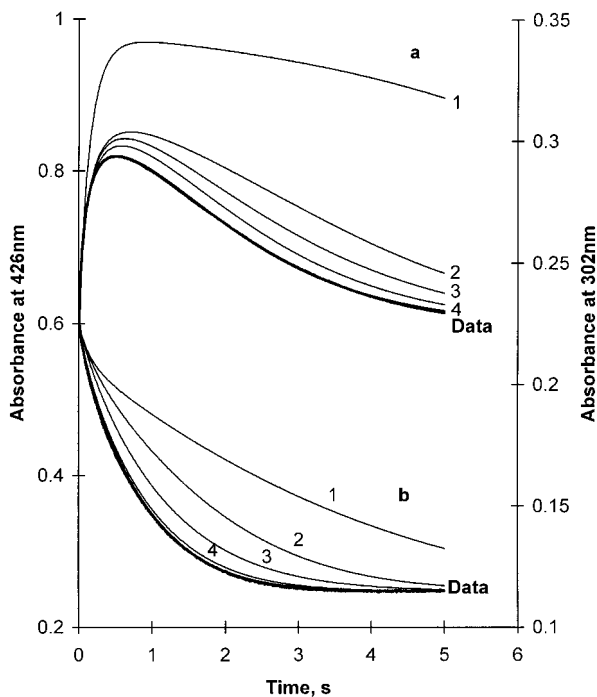


FIG. 6. Simulation of FeTMPS/ONOO⁻ catalytic system, performed using CKS software. (a) Fitting data collected at 426 nm to simulated kinetics of Fe^{III}/Fe^{IV} changes. (b) Fitting data collected at 302 nm to simulated decay of peroxyntirite. The value of k_2 used in these simulations was taken from Stern *et al.* Simulation 1 utilizes known rate constants as well as the measured rate constant for oxidation of Fe(III)TMPS, and uses the simplest mechanism, involving oxidation of Fe(III)TMPS by peroxyntirite and reduction by nitrite: $k_1 = 1 \times 10^5 \text{ M}^{-1}\text{s}^{-1}$, $k_2 = 1.4 \times 10^4 \text{ M}^{-1}\text{s}^{-1}$, $k_4 = 4.5 \times 10^8 \text{ M}^{-1}\text{s}^{-1}$, $k_{-4} = 6.9 \times 10^3 \text{ s}^{-1}$, $k_5 = 1 \times 10^3 \text{ s}^{-1}$, $k_6 = 0.2 \text{ s}^{-1}$. Simulation 2 introduces a new reduction of oxoFe(IV)TMPS step, k_7 , that utilizes nitrogen dioxide and produces nitrate, shown in Eq. [7]: $k_1 = 1 \times 10^5 \text{ M}^{-1}\text{s}^{-1}$, $k_2 = 1.4 \times 10^4 \text{ M}^{-1}\text{s}^{-1}$, $k_3 = 1.0 \times 10^7 \text{ M}^{-1}\text{s}^{-1}$, $k_4 = 4.5 \times 10^8 \text{ M}^{-1}\text{s}^{-1}$, $k_{-4} = 6.9 \times 10^3 \text{ s}^{-1}$, $k_5 = 1 \times 10^3 \text{ s}^{-1}$, $k_6 = 0.2 \text{ s}^{-1}$. Simulation 3 modifies the mechanism by adding a concerted peroxyntirite decomposition step involving oxoFe(IV)TMPS intermediate: $k_1 = 1 \times 10^5 \text{ M}^{-1}\text{s}^{-1}$, $k_2 = 1.4 \times 10^4 \text{ M}^{-1}\text{s}^{-1}$, $k_3 = 1.0 \times 10^7 \text{ M}^{-1}\text{s}^{-1}$, $k_4 = 4.5 \times 10^8 \text{ M}^{-1}\text{s}^{-1}$, $k_{-4} = 6.9 \times 10^3 \text{ s}^{-1}$, $k_5 = 1 \times 10^3 \text{ s}^{-1}$, $k_6 = 0.2 \text{ s}^{-1}$, $k_7 = 5.0 \times 10^4 \text{ M}^{-1}\text{s}^{-1}$. Simulation 4 further modifies the mechanism by introducing Fe(III)TMPS-catalyzed concerted rearrangement of peroxyntirite, shown in Eq. [8]: $k_1 = 1 \times 10^5 \text{ M}^{-1}\text{s}^{-1}$, $k_2 = 1.4 \times 10^4 \text{ M}^{-1}\text{s}^{-1}$, $k_3 = 1.0 \times 10^7 \text{ M}^{-1}\text{s}^{-1}$, $k_4 = 4.5 \times 10^8 \text{ M}^{-1}\text{s}^{-1}$, $k_{-4} = 6.9 \times 10^3 \text{ s}^{-1}$, $k_5 = 1 \times 10^3 \text{ s}^{-1}$, $k_6 = 0.2 \text{ s}^{-1}$, $k_7 = 5.0 \times 10^4 \text{ M}^{-1}\text{s}^{-1}$, $k_8 = 5.0 \times 10^4 \text{ M}^{-1}\text{s}^{-1}$.

DISCUSSION

The results, presented above, provide evidence for the participation of several reactions in the FeTMPS-catalyzed decomposition of peroxyntirite. A direct reaction of Fe(III)TMPS with ONOO⁻, similar to those observed for Mn(III)TMPyP and Fe(III)TMPyP (Eq. [1]) (33, 35), is indicated by the formation of oxo-Fe(IV)TMPS in both the catalytic and stoichiometric regimes (Fig. 3). The rate observed for this process, $k_1 = 1 \times 10^5 \text{ M}^{-1}\text{s}^{-1}$, is relatively slow compared to other metalloporphyrins. In addition, the observation

of a slow, nitrite dependent, reduction of oxoFe(IV) back to Fe(III) indicates a direct reaction between the two species (Eq. [2]). The rate of this reaction, k_2 , equal to $2 \times 10^4 \text{ M}^{-1}\text{s}^{-1}$, is considerably faster than those of oxoMn(IV)TMPyP ($140 \text{ M}^{-1}\text{s}^{-1}$) and of oxo-Fe(IV)TMPyP ($70 \text{ M}^{-1}\text{s}^{-1}$) (41). These two reactions, in concert, complete a catalytic cycle for FeTMPS. However, as illustrated in Fig. 5, the nitrite dependence of the turnover rate is very small, indicating that nitrite reduction as in Eq. [2] is a minor contributor to the overall rate.

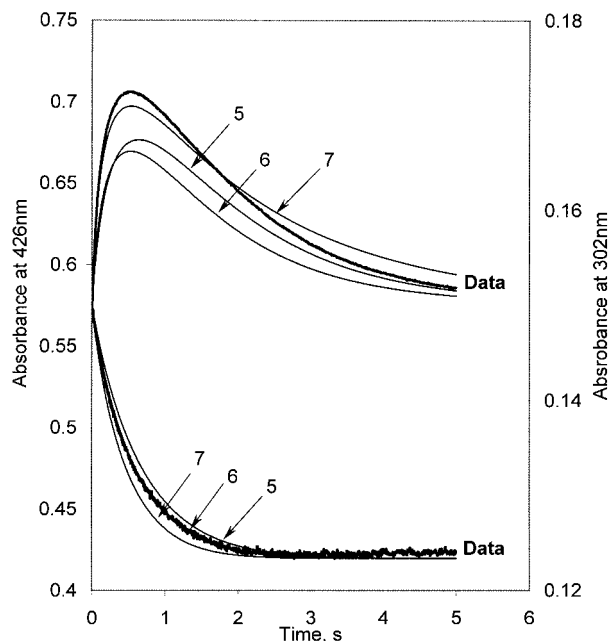
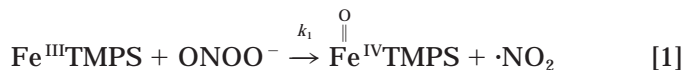
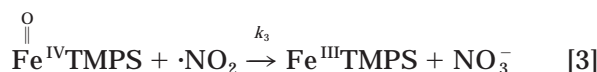


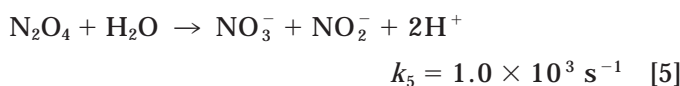
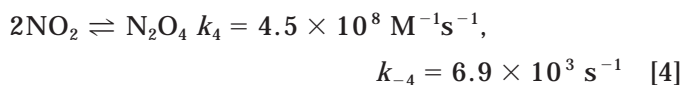
FIG. 7. Reaction of 16 μM peroxyntirite with 10 μM FeTMPS at pH 7.6 at 25°C in 100 mM phosphate buffer. Fitting data collected at 426 nm to simulated kinetics of Fe^{III}/Fe^{IV} changes and data collected at 302 nm to simulated decay of peroxyntirite. Simulation 5 utilizes same values for rate constants that were used in the Simulation 4 of catalytic decay of peroxyntirite: $k_1 = 1 \times 10^5 \text{ M}^{-1}\text{s}^{-1}$, $k_2 = 1.4 \times 10^4 \text{ M}^{-1}\text{s}^{-1}$, $k_3 = 1.0 \times 10^7 \text{ M}^{-1}\text{s}^{-1}$, $k_4 = 4.5 \times 10^8 \text{ M}^{-1}\text{s}^{-1}$, $k_{-4} = 6.9 \times 10^3 \text{ s}^{-1}$, $k_5 = 1 \times 10^3 \text{ s}^{-1}$, $k_6 = 0.2 \text{ s}^{-1}$, $k_7 = 5.0 \times 10^4 \text{ M}^{-1}\text{s}^{-1}$, $k_8 = 5.0 \times 10^4 \text{ M}^{-1}\text{s}^{-1}$. Simulation 6 utilizes values of rate constants, arrived at using the improved modeling procedure with *Scientist* software package on catalytic reaction data: $k_1 = 1.3 \times 10^5 \text{ M}^{-1}\text{s}^{-1}$, $k_2 = 1.4 \times 10^4 \text{ M}^{-1}\text{s}^{-1}$, $k_3 = 1.7 \times 10^7 \text{ M}^{-1}\text{s}^{-1}$, $k_4 = 4.5 \times 10^8 \text{ M}^{-1}\text{s}^{-1}$, $k_{-4} = 6.9 \times 10^3 \text{ s}^{-1}$, $k_5 = 1 \times 10^3 \text{ s}^{-1}$, $k_6 = 0.2 \text{ s}^{-1}$, $k_7 = 2.4 \times 10^4 \text{ M}^{-1}\text{s}^{-1}$, $k_8 = 5.4 \times 10^4 \text{ M}^{-1}\text{s}^{-1}$. Simulation 7 utilizes values that were derived by performing the fitting routine on the stoichiometric reaction data, using *Scientist* software: $k_1 = 1.75 \times 10^5 \text{ M}^{-1}\text{s}^{-1}$, $k_2 = 1.4 \times 10^4 \text{ M}^{-1}\text{s}^{-1}$, $k_3 = 1.3 \times 10^7 \text{ M}^{-1}\text{s}^{-1}$, $k_4 = 4.5 \times 10^8 \text{ M}^{-1}\text{s}^{-1}$, $k_{-4} = 6.9 \times 10^3 \text{ s}^{-1}$, $k_5 = 1 \times 10^3 \text{ s}^{-1}$, $k_6 = 0.2 \text{ s}^{-1}$, $k_7 = 2.4 \times 10^4 \text{ M}^{-1}\text{s}^{-1}$, $k_8 = 5.4 \times 10^4 \text{ M}^{-1}\text{s}^{-1}$.



It is significant that the oxidation of Fe(III)TMPS to oxoFe(IV)TMPS proceeds only to the extent of 55% even with excess peroxyxynitrite. Clearly, some reducing agent other than nitrite is present under catalytic conditions that reduces oxoFe(IV) back to Fe(III) at a rate that is comparable to the turn-over rate and very much faster than the reduction of oxoFe(IV) by nitrite. We propose that this fast reduction is a reaction of free NO_2 to afford Fe(III)TMPS and *nitrate* as indicated in Eq. [3].

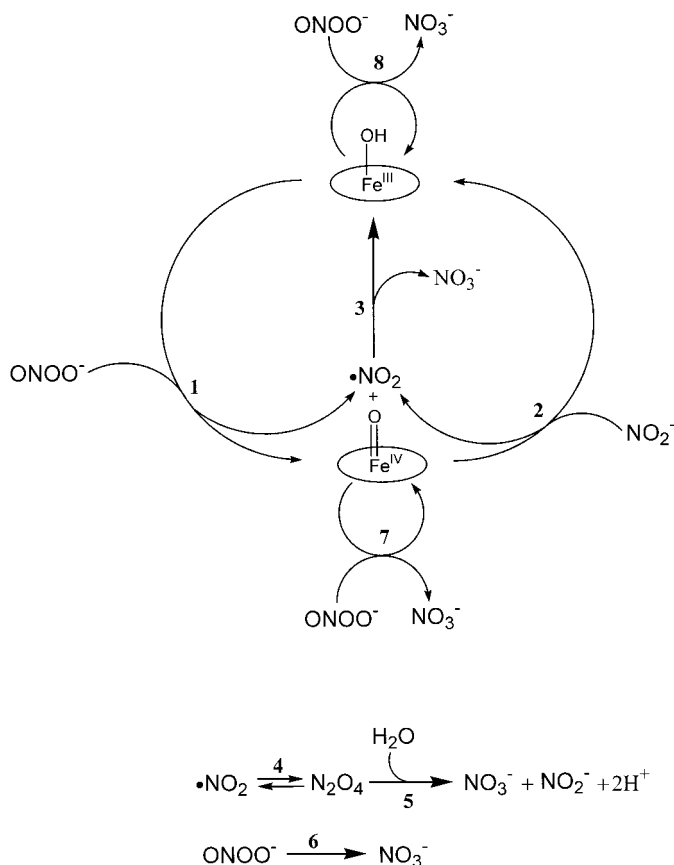


An estimate of the rate constant k_3 can be obtained from the known behavior of NO_2 in aqueous solution. The dimerization of NO_2 is fast and reversible, followed by the hydrolysis of N_2O_4 to give nitrate and nitrite according to Eqs. [4] and [5]. Overall, the hydrolysis of NO_2 proceeds with a rate constant, k_x , of $5 \times 10^7 \text{ M}^{-1}\text{s}^{-1}$. While there is no direct way to discern from the data what the rate constant of NO_2 reaction with oxoFe(IV)TMPS is, it must be competitive with NO_2 hydrolysis.



Another revealing aspect of the kinetics of the catalytic decomposition of peroxyxynitrite by FeTMPS was the observation that peroxyxynitrite decay was found to follow a single exponential throughout the course of the reaction. This is surprising when one considers that the catalyst inventory shifted from Fe(III) to 55% Fe(IV) and back to Fe(III). The simplest interpretation is that *both* the Fe(III) and Fe(IV) forms of the catalyst catalyze peroxyxynitrite decomposition at similar rates. This is in marked contrast to what we have reported for FeTMPyP (35). In that case, oxoFe(IV)TMPyP formed quickly and persisted throughout the reaction with peroxyxynitrite.

A mechanism that accounts for these observations is presented in Scheme 1. In this scheme, the primary initial process is the oxidation of Fe(III)TMPS to oxoFe(IV)TMPS and NO_2 according to Eq. [1]. The

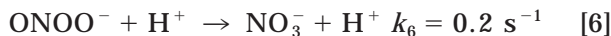


SCHEME 1. Proposed model of FeTMPS-catalyzed peroxyxynitrite decomposition.

position of the redox equilibrium between Fe(III) and Fe(IV) during catalysis is determined by the relative rate of oxidation of NO_2 by oxoFe(IV)TMPS to afford Fe(III) and nitrite (oxygen rebound) as in Eq. [2]. To explain the single exponential decay of peroxyxynitrite, a reaction of oxoFe(IV) with peroxyxynitrite to give *nitrate* is required (k_7). This process is analogous to the behavior of oxoFe(IV)TMPyP we have reported and amounts to a net rearrangement of peroxyxynitrite catalyzed by oxoFe(IV) (35). Finally, a similar rearrangement of peroxyxynitrite by Fe(III)TMPS (k_8) is included to maintain the balance that is necessary for an apparent single-exponential decay. This process can be viewed as a component of cage recombination or internal return in Eq. [1], as originally proposed by Stern *et al.* (36).

Kinetic stimulations. A quantitative assessment of the relative importance of the several pathways in Scheme 1 was obtained by a series of kinetic simulations using Chemical Kinetics Simulator (CKS) that employs a rigorously accurate stochastic algorithm to propagate reactions (42, 43). The rates of Fe(III)TMPS oxidation by peroxyxynitrite (k_1) and the reduction of oxoFe(IV)TMPS by nitrite were fixed to the experimen-

tal values. Likewise, the rates of hydrolysis of N_2O_4 (Eqs. [4] and [5]) and the spontaneous decay of peroxy nitrite, Eq. [6], were fixed to literature (35) and measured values, respectively.



When our system was simulated using the reactions, mentioned above, it becomes apparent that our description of the system is incomplete as can be judged from Simulation 1 in Fig. 6. The simulation predicts the maximum yield of oxoFe(IV) to be 88% and to persist for too long. It also predicts the decay of ONOO^- to occur with $t_{1/2}$ of 1.72 s, compared to the observed $t_{1/2}$ of 0.55 s. This means that the catalytic cycle of Eqs. [1] and [2] is too slow and that there must be another reaction to describe reduction of oxoFe(IV) to Fe(III).

We have considered several reactive species, present in our system, as possible fast oxoFe(IV)TMPS reductants: hydrogen peroxide, peroxy nitrite, dinitrogen tetroxide, and nitrogen dioxide. All but NO_2 , were deemed as insignificant in our catalytic system based on the following series of analyses.

Hydrogen peroxide is present in our ONOO^- preparations as a $\sim 10\%$ impurity. It has been shown (41) that it can reduce oxoMn(IV)TMPyP to Mn(III)TMPyP, albeit, at a very slow rate, $1100 \text{ M}^{-1}\text{s}^{-1}$ and that it may also reduce other manganese porphyrins from +4 to +3 oxidation states (44). Having measured both the oxidation rate of Fe(III)TMPS by H_2O_2 and the rate of reaction of H_2O_2 with oxoFe(IV)TMPS and found these to be 240 and $10 \text{ M}^{-1}\text{s}^{-1}$, respectively, we can exclude hydrogen peroxide as an important reactant in our system due to its low reactivity and micromolar concentrations in this catalytic system.

An alternative fast reduction step, involving oxidation of peroxy nitrite by oxoFe(IV) has also been suggested (45). Extensive computer simulations, where peroxy nitrite was used instead of nitrogen dioxide to reduce oxoFe(IV)TMPS, have given much poorer fits in our catalytic system. Also, since in this case both reduction and oxidation of FeTMPS would depend on peroxy nitrite concentration then the Fe(III)/Fe(IV) ratio would be independent of the initial ONOO^- concentration. However, we found that this ratio is indeed dependent on ONOO^- concentration. Third, reduction of oxoFe(IV) by peroxy nitrite would yield peroxy nitrite radical. Peroxy nitrite radical would either decompose to NO and O_2 or react with itself. In either case, the final product would be nitrite and O_2 . If this were the case, then the major product from the catalytic decomposition of ONOO^- by FeTMPS would be nitrite, but Stern *et al.* (36) have shown that the major product is nitrate. We can conclude that in our catalytic system

the reduction of oxoFe(IV)TMPS by ONOO^- is insignificant.

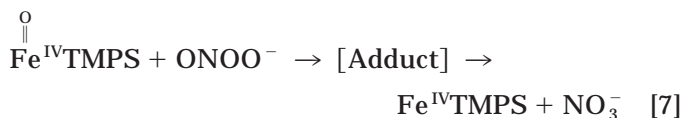
Another possible reducing agent is N_2O_4 , formed from fast dimerization of nitrogen dioxide. However, N_2O_4 , upon its formation, undergoes solvent-assisted hydrolysis to nitrite and nitrate at an exceptionally fast first-order rate of 100 s^{-1} (k_5). Our simulations have shown that N_2O_4 is a fleeting intermediate, whose steady-state concentrations during reactions are nanomolar. The reaction rate would have to exceed diffusion-controlled limit to have a significant effect on reduction of oxoFe(IV)TMPS. Simulations, where reaction of NO_2 with oxoFe(IV)TMPS was replaced with the reaction of N_2O_4 at rates up to $10^{10} \text{ M}^{-1}\text{s}^{-1}$, showed that N_2O_4 was not able to reduce Fe(IV) fast enough. This analysis shows that N_2O_4 is not an important reducing agent in our system.

Since, NO_2 is present in near steady state concentrations throughout the reaction, and because both oxoFe(IV) and NO_2 are reactive species, we invoked a reaction between the two species, described by Eq. [3], that produces nitrate while reducing oxoFe(IV). This *oxygen atom transfer-coupled single electron reduction* reaction may contain several elementary steps where the nitrogen dioxide first bonds to the oxygen of oxoFe(IV), giving nitrato-Fe(III), followed by dissociation of nitrate from the metal. This reaction would represent the fast reduction of oxoFe(IV)TMPS that is required by the kinetic behavior.

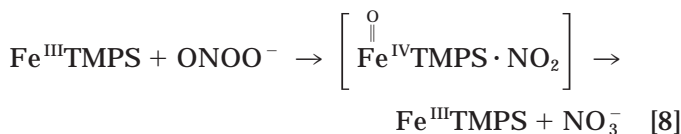
It was found that the predicted maximum ratio of oxoFe(IV)TMPS to Fe(III)TMPS was very sensitive to the rate constant chosen for oxygen rebound to NO_2 (k_3). This rate constant must be similar in magnitude to that of overall NO_2 hydrolysis, $k_x = 5 \times 10^7 \text{ M}^{-1}\text{s}^{-1}$. Thus, we estimated k_3 to be between 10^5 and $10^9 \text{ M}^{-1}\text{s}^{-1}$ and used computer simulations to arrive at the value that gives better fit of the data in terms of the maximum yield and time of formation of oxoFe(IV). The value obtained for the rate constant of the reaction in Eq. [3] is $k_3 = 1 \times 10^7 \text{ M}^{-1}\text{s}^{-1}$. This value for k_3 is reasonable since it is slower than the rate constant of NO_2 dimerization and because many radical recombination reaction are known to occur at similar and faster rates.

Introduction of oxygen rebound to NO_2 (Eq. [3]) allowed us to simulate the changes in the FeTMPS inventory very well. However, the experimental ONOO^- decay still occurred faster than our simulation predicted as seen in Simulation 2 in Fig. 6. Also, we know that levels of Fe(III) and oxoFe(IV) vary greatly in the course of the reaction, and yet the decay of ONOO^- is monophasic since it can be fitted to a single exponential fairly well as can be seen from Fig. 1, suggesting that both Fe(III)- and Fe(IV)-dependent catalytic paths operate at similar rates. This observation indicates that we are missing at least one more reaction. From earlier

work by Lee *et al.* (35) on FeTMPyP, we know that oxoFe(IV) species is a plausible catalytic agent, so it is likely that in our system oxoFe(IV)TMPS is also acting as a peroxyxynitrite catalyst. If only oxoFe(IV) was catalytic then we would not expect of the ONOO⁻ decay curve to be monophasic because the oxoFe(IV) catalytic path would become dominant and the ONOO⁻ decay curve would change shape. We do not see that, in fact the rate of decay of peroxyxynitrite was unaffected by the changing ratio of Fe(III)TMPS to oxoFe(IV)TMPS and that suggests that both Fe(III)TMPS and oxoFe(IV)TMPS may act as "internal return" catalysts. Reaction of oxoFe(IV) with peroxyxynitrite, represented by Eq. [7], can be understood as one of the possible reactions described by Lee *et al.* (35). One such possibility is that oxoFe(IV) and ONOO⁻ form an adduct that decomposes to oxoFe(IV) and nitrate.



The Fe(III)TMPS reaction with peroxyxynitrite is shown in Eq. [8] and can be understood as an initial formation of a caged radical pair, and an internal return of NO₂, that produces Fe(III) and nitrate in a manner suggested by Stern *et al.* (36). However, diffusion of NO₂, hydrolysis, and reencounter with oxoFe(IV)TMPS are also occurring (Scheme 1).



More so, the two reactions should have a similar rate constant because, once again, we do not see any unpredicted changes in the slope of the ONOO⁻ decay curve. We assumed the two rates to be approximately equal. When we add these two reactions to our model, and optimize the two rate constants, k_7 and k_8 , we get a value of $5 \times 10^4 \text{ M}^{-1}\text{s}^{-1}$ for each as seen in Simulation 3 and 4 in Fig. 6. Addition of these two reactions to our scheme does not affect the changes in the catalyst inventory, but it greatly improves the fit to the peroxyxynitrite decay data.

The mechanism, proposed in Scheme 1, accounts for all of the observations and the rate constants are consistent with the computer modeling studies. The data supports that the catalytic cycle is initiated by a reaction of peroxyxynitrite with the iron porphyrin. Upon binding and subsequent O—O bond homolysis, oxoFe(IV) and NO₂ species are produced. At this point, several things may happen. It is possible that initially

oxoFe(IV) and NO₂ are a caged-radical pair. An internal return would occur if nitrogen dioxide were able to rebound with the metal before diffusing away, producing nitrate and Fe(III) porphyrin. This is represented by Eq. [8]. If nitrogen dioxide escapes the radical cage, it can dimerize, producing N₂O₄, which can subsequently decompose into nitrite and nitrate, represented by Eqs. [4] and [5]. It may also encounter and react with another oxoFe(IV) porphyrin molecule, reducing and metal center to Fe(III) and producing nitrate in the process, represented by Eq. [3]. The oxoFe(IV) porphyrin by itself may also catalytically react with a peroxyxynitrite molecule, converting it to nitrate, in a fashion similar to FeTMPyP. This is accounted for by Eq. [7]. Our model so far has neglected several considerations such as ligand exchange (46), protonation (37), aggregation (47), which may take place to some extent in our catalytic system. We therefore omitted these from our treatment in favor of a simpler model that describes main reaction paths that are present.

Finally, we carried out another series of simulations of FeTMPS-catalyzed peroxyxynitrite decay, utilizing Scientist software (Micromath, Inc.), which contains numerical integration package Episode, for solving systems of stiff differential equations. This software allowed us to fit our model to the data and statistically evaluate fitted parameters. The modeling was performed using Eqs. [1] through [8], where rate constants k_2 , k_{4a} , k_{4b} , k_5 , and k_6 were held constant, while k_1 , k_3 , k_7 , k_8 , and $[\text{NO}_2^-]$ were allowed to vary within very narrow limits since there was an uncertainty in the exact value of these parameters. The model was fitted simultaneously to FeTMPS and peroxyxynitrite decay data using least-squared minimization routine. The best fit was obtained when the value of k_1 was $1.29 \times 10^5 \text{ M}^{-1}\text{s}^{-1}$, k_3 was $1.68 \times 10^7 \text{ M}^{-1}\text{s}^{-1}$, k_7 was $2.4 \times 10^4 \text{ M}^{-1}\text{s}^{-1}$, and k_8 was $5.5 \times 10^4 \text{ M}^{-1}\text{s}^{-1}$. The initial nitrite concentration was 21 μM, corresponding to 33% of the initial peroxyxynitrite concentration. The goodness of fit (R^2) was determined to be 0.99999 for both data sets. Several simulations were performed in which k_7 and k_8 were alternatively set to zero. When one constant was set to zero, the program readjusted the other constant, accordingly, to compensate for the change. The goodness of fit was not reduced as a result of this procedure, suggesting that the two rate constants cannot be distinguished by simulation analysis. However, setting both k_7 and k_8 to zero reduced the quality of the fit and changed the values of k_1 and k_3 above experimentally determined estimates, implying that either reaction 7 or 8 or both are necessary. Values for the unknown rate constants obtained in this modeling study differ slightly from the values obtained previously, using CKS software. However, since these values gave better

fits, they were deemed more accurate and were thus reported as the final values.

In addition to simulating the catalytic reaction, the stoichiometric reaction between 16 μM peroxyxynitrite and 10 μM Fe(III)TMPS was simulated and fitted, as shown in Fig. 7. When the values for rate constants, obtained in the previous simulation, were used to simulate stoichiometric reaction, Simulations 5 and 6, the resulting traces did not fit as well to the data ($R^2 = 0.997$ and 0.994 for 426 and 302 nm data, respectively, for Simulation 5). To obtain a better fit, the values of k_1 and k_3 as well as the initial nitrite concentration were allowed to vary. The best fit was obtained when k_1 was $1.75 \times 10^5 \text{ M}^{-1}\text{s}^{-1}$ and k_3 was $1.3 \times 10^7 \text{ M}^{-1}\text{s}^{-1}$ at 30 μM nitrite, a modest change. This gave the R^2 value of 0.9997 for the data set. The values obtained from simulations of two sets of reaction conditions are sufficiently close to suggest that the proposed model and the derived rate constants are correct.

Reactant flux analysis of FeTMPS- and FeTMPyP-catalyzed peroxyxynitrite decay. Using our proposed mechanism and rate constants for FeTMPS and the mechanism and the rate constants for FeTMPyP catalysis, obtained by Lee *et al.* (35), as well as utilizing our simulation data, we were able to determine the fluxes of several species through various reactions paths. The results of our analysis are shown in Table I. For example, the total flux of peroxyxynitrite, decomposed by Reaction 7, during its FeTMPS-catalyzed decay was determined as follows. The instantaneous reaction rate at each time point was obtained by multiplying the rate constant for Reactions 7 by the concentrations of peroxyxynitrite and Fe(IV)TMPS at each time point. Then this instantaneous reaction rate was numerically integrated over the whole reaction time, using the Newton method. The analysis was performed for both FeTMPS and FeTMPyP and allowed direct comparison of both catalysts. In the presence of 10 μM FeTMPS, 53.7% of the 66 μM peroxyxynitrite was decomposed by Reaction 1, the source of nitrogen dioxide radicals, while only 15.1% was decomposed by Reaction 6, the background self-decay. At the same time, 8.3 and 22.8% of peroxyxynitrite was decomposed by the Fe(IV)TMPS-adduct and Fe(III)TMPS internal return reactions, respectively. The reduction Fe(IV)TMPS occurs via Reactions 2 and 3. The analysis has shown that only 14.8% of Fe(IV)TMPS was reduced by the nitrite-dependent Reaction 2, while 85.2% of Fe(IV)TMPS was captured by the nitrogen dioxide radicals via Reaction 3 to give Fe(III)TMPS and nitrate.

The background decay of peroxyxynitrite via protonation and rearrangement (Reaction 6) has been shown to yield significant levels (up to 50%) of nitrite above pH 8. Under our conditions, at pH 7.4, the yield of nitrite, which plays an important role in the redox balance of

TABLE I
Analysis of Peroxyxynitrite Decay Pathways

Reaction	FeTMPS		FeTMPyP ^a	
	Rate constant, $\text{M}^{-1}\text{s}^{-1}$	Total flux, μM	Rate constant, $\text{M}^{-1}\text{s}^{-1}$	Total flux, μM
1	1.3×10^5	35.45	5.0×10^7	10.2
2	1.4×10^4	5.24	73	5.96
3	1.7×10^7	30.21	—	—
6 ^b	0.2	10.00	0.2	6.18
7	2.4×10^4	5.49	1.8×10^6	55.2
8	5.4×10^4	15.06	—	—
Percentage fluxes of peroxyxynitrite				
Reaction 1		53.7%		15.4%
Reaction 6		15.1%		0.9%
Reaction 7		8.3%		83.6%
Reaction 8		22.8%		—
Percentage fluxes of Fe(IV)				
Reaction 2		14.8%		100.0%
Reaction 3		85.2%		—

Note. Total concentrations of peroxyxynitrite consumed by each reaction (Total Flux) were calculated from the known rate constants and concentrations of peroxyxynitrite, obtained from simulations. From this data, fractions of the total peroxyxynitrite consumed by each individual reaction (Percentage Flux) were calculated. The following initial conditions were used in the simulations and in the flux analysis: Iron (III) porphyrins were 10 μM , peroxyxynitrite was 66 μM , and nitrite was 20 μM .

^a Rate constants are from Ref. 35.

^b Rate constant has units of s^{-1} .

the catalyst, from this background reaction has been omitted as a very minor contribution. Since the initial level of nitrite was determined to be $\sim 20 \mu\text{M}$ and because Reaction 6 accounts for only 15.1% of peroxyxynitrite decay, the amount of nitrite formed by this reaction will constitute only 3–8% of total nitrite. Since the nitrite-dependent reduction of oxoFe(IV)TMPS itself accounts for only 14.8%, the increased level of nitrite would have marginal effect on the concentrations of the catalysts.

By contrast, the analysis of the FeTMPyP-catalyzed peroxyxynitrite decay showed that 83.6% of peroxyxynitrite was decomposed by an analogue of Reaction 7, which was proposed earlier. The background spontaneous decay of peroxyxynitrite accounted for only 0.9% of total peroxyxynitrite decay, while the oxidation of Fe(III)TMPyP by peroxyxynitrite, Reaction 1, used by 15.4% of the peroxyxynitrite. This explains the low nitrite/nitrate ratio observed by Stern *et al.* (36) in case of FeTMPyP since the only nitrite producing step is dimerization and hydrolysis of nitrogen dioxide produced by Reaction 1. At higher peroxyxynitrite concentrations, this ratio is expected to decrease even more since only one

equivalent of peroxyxynitrite is required to convert Fe(II)TMPyP to oxoFe(IV)TMPyP due to lack of fast reduction reactions. In such a case most of catalytic decomposition of peroxyxynitrite would be carried out by the reactive intermediate, Fe(IV)TMPyP, that does not yield any nitrite.

Conclusion. When we initiated our work on FeTMPS, we wanted to determine if there were mechanistic reasons for its reported higher biological activity (30, 31), compared to FeTMPyP, which we have studied previously (35). Intrinsic rates of reaction of FeTMPS with peroxyxynitrite are much slower than those of FeTMPyP and yet it is more active *in vivo*. This, of course, may be due to pharmacokinetics or differential tissue distribution, but we have shown here that the reactions FeTMPS with peroxyxynitrite are chemically distinct from those of FeTMPyP in several aspects. OxoFe(IV)TMPS was found to react efficiently with both nitrite ($k_2 = 2 \times 10^4 \text{ M}^{-1}\text{s}^{-1}$) and nitrogen dioxide ($k_3 = 1.7 \times 10^7 \text{ M}^{-1}\text{s}^{-1}$), yielding the reduced form of the catalyst while these processes are slow for oxoFe(IV)TMPyP. This could be very significant *in vivo* since oxoFe(IV)TMPS would be expected to lower the steady-state concentration of NO_2 and, thus, decrease the amount of peroxyxynitrite-induced tyrosine nitration (48). For the case of FeTMPyP, the oxoFe(IV) catalytic pathway (Eq. [7]) is clearly evident and necessary to explain slower apparent turnover at higher peroxyxynitrite concentrations (35). However, with FeTMPS, the Fe(III) and Fe(IV) forms of the catalyst react with peroxyxynitrite at similar rates. This fact made the FeTMPS system much more difficult to deconvolute, compared to FeTMPyP, which had large differences in the rates of reaction of Fe(III) versus oxoFe(IV) catalysts.

This remarkable diversity of reactivity arises apparently from the electronic and steric effects that a porphyrin ligand imposes on the metal center. In the case of FeTMPyP, the porphyrin ligand is positively charged and is very flat as seen from a molecular modeling of the porphyrin using software by Cache Scientific. This allows easy access of solvent and other molecules to the metal center. In the case of FeTMPS, the ligand is negatively charged and is very sterically hindered. As a result of that, the porphyrin is more twisted and the access to the metal center is limited by the steric bulk of the porphyrin substituents. Also, the methyl groups on the phenyl rings are located above and below the metal center, creating a hydrophobic cavity. This may explain why FeTMPS reacts faster with radicals, compared to FeTMPyP. Also, the pyridinium groups in FeTMPyP are electron withdrawing and they make the metal center electron-deficient and very reactive, whereas ligand in FeTMPS is neither electron withdrawing nor donating, which makes the metal center

relatively less reactive. This may explain why intrinsic rates of reaction of FeTMPS with molecules in our system are slower than those of FeTMPyP.

The current study of FeTMPS reactivity toward peroxyxynitrite and previous studies of FeTMPyP and other porphyrins show that metal porphyrins are versatile catalysts of peroxyxynitrite reactions with varied catalytic abilities and mechanisms. Modifications of the porphyrin ligands introduce not only changes in the rates of reaction but may also change the mechanisms of action. Understanding the mechanistic details of peroxyxynitrite decomposition catalysis and relating these aspects to varied structures of the catalyst will provide a better understanding of structure–function relationships and will also lead to design of better, more efficient peroxyxynitrite catalysts.

ACKNOWLEDGMENTS

We thank National Institutes of Health (GM 36298) for financial support. We also thank Dr. Michael Stern, Dr. James Bourassa for insightful discussions, and Ning Jin and Dr. Jinbo Lee for technical help with stopped-flow kinetics.

REFERENCES

1. Beckman, J. S., Estevez, A. G., Spear, N., Manuel, S. M., Radi, R., Henderson, C., and Barbeito, L. (1998) *J. Neurosci.* **18**, 923–939.
2. Bohle, D. S. (1998) *Curr. Opin. Chem. Biol.* **2**, 194–200.
3. Cookson, M. R., and Shaw, P. J. (1999) *Brain Pathol.* **9**, 165–186.
4. Radi, R., Beckman, J. S., Bush, K. M., and Freeman, B. A. (1991) *Arch. Biochem. Biophys.* **288**, 481–487.
5. Groves, J. T. (1999) *Curr. Opin. Chem. Biol.* **3**, 226–235.
6. Klebanoff, S. J. (1993) *Free Rad. Biol. Med.* **14**, 351–360.
7. Lin, K.-T., Xue, J.-Y., Nomen, M., Spur, B., and Wong, P. Y.-K. (1995) *J. Biol. Chem.* **270**, 16487–16490.
8. Parker, D., Parker, T. A., Town, T., Suo, Z., Fang, C., Humphrey, J., Crawford, F., and Mullan, M. (1998) *Exp. Neurol.* **152**, 116–122.
9. Gardner, P. R., Constantino, G., Szabo, C., and Salzman, A. L. (1997) *J. Biol. Chem.* **272**, 25071–25076.
10. Radi, R., Rodriguez, M., Castro, L., and Telleri, R. (1994) *Arch. Biochem. Biophys.* **308**, 89–95.
11. Radi, R., Castro, L., and Rodriguez, M. (1994) *J. Biol. Chem.* **269**, 29409–29415.
12. Radi, R., and Cassina, A. (1996) *Arch. Biochem. Biophys.* **328**, 309–316.
13. Radi, R., Beckman, J. S., Bush, K. M., and Freeman, B. A. (1991) *J. Biol. Chem.* **266**, 4244–4250.
14. Shi, X., Rojanasakul, Y., Gannett, P., Liu, K., Mao, Y., Daniel, L. N., Ahmed, N., and Saffiotti, U. (1994) *J. Inorg. Biochem.* **56**, 77–86.
15. Beckman, J. S., Ischiropoulos, H., Zhu, L., van der Woerd, M., Smith, C., Chen, J., Harrison, J., Martin, J. C., and Tsai, M. (1992) *Arch. Biochem. Biophys.* **298**, 438–445.
16. Beckman, J. S., Ischiropoulos, H., Zhu, L., Chen, J., Tsai, M.,

- Martin, J. C., and Smith, C. D. (1992) *Arch. Biochem. Biophys.* **298**, 431–437.
17. Pryor, W. A., Uppu, R. M., Lemerceir, J.-N., Squadrito, G. L., Zhang, H., and Bolzan, R. M. (1998) *Arch. Biochem. Biophys.* **358**, 1–16.
18. Keyer, K., and Imlay, J. A. (1997) *J. Biol. Chem.* **272**, 27652–27659.
19. Patel, M. (1998) *J. Neurochem.* **71**, 1068–1074.
20. Reist, M., Jenner, P., and Halliwell, B. (1997) *FEBS Lett.* **423**, 231–234.
21. Salvemini, D., Riley, D. P., Lennon, P. J., Wang, Z.-Q., Currie, M. G., MacArthur, H., and Misko, T. P. (1999) *Br. J. Pharmacol.* **127**, 685–692.
22. Goldstein, S., and Czapski, G. (1998) *J. Am. Chem. Soc.* **120**, 3458–3463.
23. Houk, K. N., Condorski, K. R., and Pryor, W. A. (1996) *J. Am. Chem. Soc.* **118**, 13002–13006.
24. Radi, R. (1998) *Chem. Res. Toxicol.* **11**, 720–721.
25. Squadrito, G. L., and Pryor, W. A. (1998) *Chem. Res. Toxicol.* **11**, 718–719.
26. Houk, K. N., Bartberger, M. D., and Olson, L. P. (1998) *Chem. Res. Toxicol.* **11**, 710–711.
27. Ingold, K. U., Richeson, C. E., Mulder, P., and Bowry, V. W. (1998) *J. Am. Chem. Soc.* **120**, 7211–7219.
28. Koppenol, W. H., Kissner, R., Nauser, T., Bugnon, P., and Lye, P. G. (1997) *Chem. Res. Toxicol.* **10**, 1285–1292.
29. Pryor, W. A., Goldstein, S., Squadrito, G. L., and Czapski, G. (1996) *Free Rad. Biol. Med.* **21**, 965–974.
30. Misko, T. P., Highkin, M. K., Veenhuizen, A. W., Manning, P. T., Stern, M. K., Currie, M. G., and Salvemini, D. (1998) *J. Biol. Chem.* **273**, 15646–15653.
31. (a) Misko, T. P., Salvemini, D., Wang, Z.-Q., Stern, M. K., and Currie, M. G. (1998) *Proc. Natl. Acad. Sci. USA* **95**, 2659–2663. (b) Salvemini, D., Cuzzocrea, S., Misko, T. P., Costantino, G., Mazzon, E., Micali, A., Caputi, A. P., and MacArthur, H. (2000) *FASEB J.* **14**, 1061–1072.
32. Balavoine, G. G. A., Geletii, Y. V., and Bejan, D. (1997) *Nitric Oxide* **1**, 507–521.
33. Groves, J. T., Lee, J., and Hunt, J. A. (1997) *Bioorg. Med. Chem. Lett.* **7**, 2913–2918.
34. Groves, J. T., Hunt, J. A., and Lee, J. (1997) *Chem. Biol.* **4**, 845–858.
35. Groves, J. T., Lee, J., and Hunt, J. A. (1998) *J. Am. Chem. Soc.* **120**, 7493–7501.
36. Stern, M. K., Jensen, M. P., and Kramer, K. (1996) *J. Am. Chem. Soc.* **118**, 8735–8736.
37. Miskelly, G. M., and La, T. (1995) *J. Am. Chem. Soc.* **117**, 3613–3614.
38. White, R., Crow, J., Spear, N., Thomas, S., Patel, R., Green, I., Beckman, J., and Darley-Usmay, V. (1996) in *Methods in Molecular Biology* (Titheradge, M. A., Ed.), Vol. 100, pp. 215–230, Humana, Totowa.
39. Czapski, G., Saha, A., Goldstein, S., and Cabelli, D. (1998) *Free Rad. Biol. Med.* **24**, 653–659.
40. Tannenbaum, S. R., Green, L. C., Wagner, D. A., Glogowski, J., Skipper, P. L., and Winshok, J. S. (1982) *Anal. Biochem.* **126**, 131–138.
41. Lee, J. (1998) 1. Manganese and Iron Porphyrin Probes of the Chemistry and Biology of Peroxynitrite. 2. Biomimetic Transmembrane Allosteric A Molecular Light Switch. Ph.D. Thesis, Princeton University.
42. Bunker, D. L., Garrett, B., Kliendienst, T., and III, G. S. L. (1974) *Combust. Flame* **23**, 373.
43. Gillespie, D. T. (1976) *J. Comput. Phys.* **22**, 403.
44. Crow, J. P. (1999) *Arch. Biochem. Biophys.* **371**, 41–52.
45. Herold, S., Mehl, M., Daiber, A., Shoun, H., and Ullrich, V. (1999) *Nitric Oxide* **3**, 142–152.
46. Fridovich, I., Batinic-Haberle, I., Spasojevic, I., Hambright, P., Benov, L., and Crumbliss, A. L. (1999) *Inorg. Chem.* **38**, 4011–4022.
47. Dancil, K.-P. S., Hilario, L. F., Khoury, R. G., Mai, K. U., Nguyen, C. K., Weddle, K. S., and Shachter, A. M. (1997) *J. Heterocycl. Chem.* **34**, 749–755.
48. Hurst, J. K., and Jiang, Q. (1997) *J. Biol. Chem.* **272**, 32767–32772. [The ability of FeTMPS to inhibit nitration was tested, using fluorescein as a probe for peroxynitrite-induced nitration. When 25 μ M peroxynitrite was reacted with 5 μ M fluorescein in presence of 5 μ M FeTMPS, the yield of nitration was determined to be 20%, based on substrate. But, in absence of FeTMPS, the yield of nitrofluorescein was 33%. The yields were determined spectrophotometrically.]
49. Hurst, J. K., Lyman, S. V., and Coddington, J. W. (1999) *J. Am. Chem. Soc.* **121**, 2438–2443.